The Astrophysical Journal, 657:609–617, 2007 March 1
© 2007. The American Astronomical Society. All rights reserved. Printed in U.S.A.

Lyα ABSORPTION FROM HELIOSHEATH NEUTRALS

Brian E. Wood,[1] Vladislav V. Izmodenov,[2,3] Jeffrey L. Linsky,[1] and Yury G. Malama[3]
Received 2006 August 18; accepted 2006 November 13

ABSTRACT

We assess the information that *HST* observations of stellar Lyα lines can provide on the heliosheath, the region of the heliosphere between the termination shock and heliopause. To search for evidence of heliosheath absorption, we conduct a systematic inspection of stellar Lyα lines reconstructed after correcting for ISM absorption (and heliospheric/astrospheric absorption, if present). Most of the stellar lines are well centered on the stellar radial velocity, as expected, but the three lines of sight with the most downwind orientations relative to the ISM flow (χ^1 Ori, HD 28205, and HD 28568) have significantly blueshifted Lyα lines. Since it is in downwind directions that heliosheath absorption should be strongest, the blueshifts are almost certainly caused by previously undetected heliosheath absorption. We make an initial comparison between the heliosheath absorption and the predictions of a pair of heliospheric models. A model with a complex multicomponent treatment of plasma within the heliosphere predicts less absorption than a model with a simple single-fluid treatment, which leads to better agreement with the data. Finally, we find that nonplanetary energetic neutral atom (ENA) fluxes measured by the ASPERA-3 instrument on board *Mars Express*, which have been interpreted as being from the heliosheath, are probably too high to be consistent with the relative lack of heliosheath absorption seen by *HST*. This would argue for a local interplanetary source for these ENAs instead of a heliosheath source.

Subject headings: hydrodynamics — interplanetary medium — solar wind — ultraviolet: stars

1. INTRODUCTION

Ultraviolet observations of nearby stars from the *Hubble Space Telescope* (*HST*) have unexpectedly proven to be very useful for studying the outermost heliosphere. High-resolution spectra of the H I Lyα line at 1215.67 Å sometimes show signatures of absorption from H I in the heliosphere in cases where the interstellar absorption is weak enough to allow the heliospheric signal to be detectable (Wood et al. 2005b). Absorption is also sometimes observed from the astrosphere of the observed star, which has provided the first detections and measurements of winds from solar-like stars (Wood et al. 2005a).

Figure 1 shows a picture of the basic heliospheric structure, which is characterized by three sharp boundaries (see, e.g., Zank 1999). The innermost is the termination shock, where the solar wind is decelerated to subsonic speeds. Then there is the heliopause, which separates the plasma flows of the fully ionized solar wind and partially ionized interstellar medium (ISM). Although the charged constituents of the ISM cannot penetrate the heliopause, the neutral atoms in the ISM flow can. The outermost boundary is the bow shock, where the ISM flow is decelerated to subsonic speeds (see, e.g., Zank 1999). The *Voyager 1* satellite, which is traveling close to the upwind direction of the ISM flow seen by the Sun, recently crossed the termination shock at a distance of 94 AU from the Sun (Stone et al. 2005), roughly consistent with the model predictions in Figure 1.

For most lines of sight, the Lyα absorption from heliospheric H I will be dominated by the so-called hydrogen wall region between the heliopause and bow shock (region 3 in Fig. 1), where models predict that interstellar H I will be heated, compressed, and decelerated after crossing the bow shock (Baranov et al. 1991; Baranov & Malama 1993, 1995; Zank et al. 1996). There are currently a total of eight detections of heliospheric absorption. All but one are in upwind directions. To be more precise, if we define θ to be the angle between the observed line of sight and the upwind direction of the ISM flow vector seen by the Sun, all but one of the lines of sight with detected heliospheric absorption have $\theta < 75^\circ$ (Wood et al. 2005b). This is consistent with model predictions, which demonstrate that the deceleration of H I within the hydrogen wall relative to the ISM flow is strongest in upwind directions. This helps to separate the heliospheric absorption from the ISM absorption, making the heliospheric signal easier to detect.

Neutrals within the heliosphere interact with other particles almost entirely via charge exchange, densities being too low for thermal particle collisions to be important. The population of hydrogen wall H I that dominates Lyα absorption in upwind directions is formed by charge exchange between interstellar H I that has passed unimpeded through the bow shock and ISM protons that have been heated, decelerated, and compressed at the bow shock. However, interstellar neutrals can also penetrate the heliopause and charge exchange with solar wind protons in the heliosheath region in between the termination shock and heliopause (region 2 in Fig. 1). Downwind lines of sight that look through the tail of the heliosphere will have extended path lengths through the heliosheath. The Lyα absorption in such directions, if it can be detected, will potentially be dominated by the heliosheath rather than the hydrogen wall.

In this paper, we focus on observations and model predictions concerning Lyα absorption from heliosheath neutrals. There are several reasons why this is useful. One is simply that heliosheath absorption probes a different region of the heliosphere than the hydrogen wall absorption that dominates nearly all previous detections of heliospheric and astrospheric Lyα absorption. Another reason is that hydrodynamic models of the heliosphere that use a fully kinetic treatment of the neutrals seem to predict a disturbingly large amount of heliosheath absorption in downwind directions, which may be in conflict with nondetections of absorption in those directions (Wood et al. 2000; Izmodenov et al.

[1] JILA, University of Colorado, Boulder, CO; woodb@origins.colorado.edu, jlinsky@jila.colorado.edu.
[2] Lomonosov Moscow State University, Department of Aeromechanics and Gas Dynamics, Moscow, Russia; izmod@ipmnet.ru.
[3] Space Research Institute (IKI) RAS, and Institute for Problems in Mechanics RAS, Prospect Vernadskogo, Moscow, Russia.

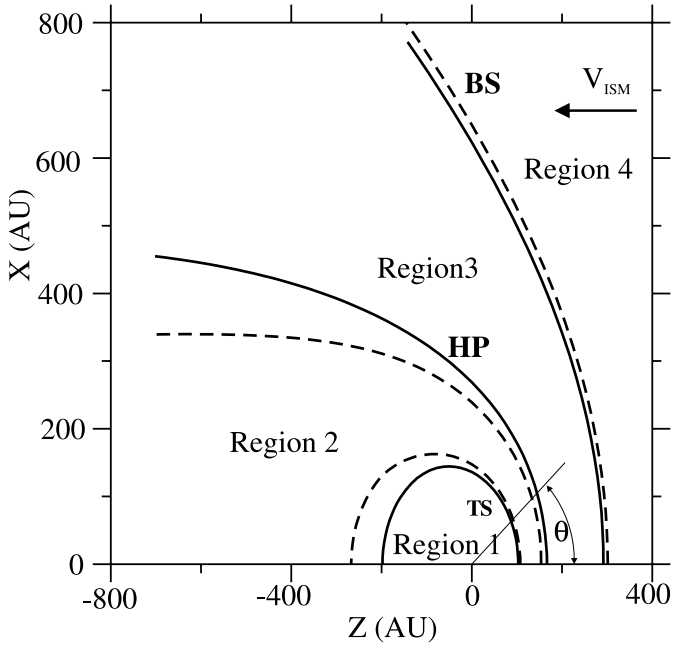

FIG. 1.—Locations of the termination shock (TS), heliopause (HP), and bow shock (BS) according to the single-fluid (*solid lines*) and multicomponent (*dashed lines*) plasma models used in the text (see § 2.1 and § 3). The Sun is at the origin. The ISM flow direction is indicated by the V_{ISM} vector, and the angle with respect to the upwind direction of this flow angle, θ, is also illustrated.

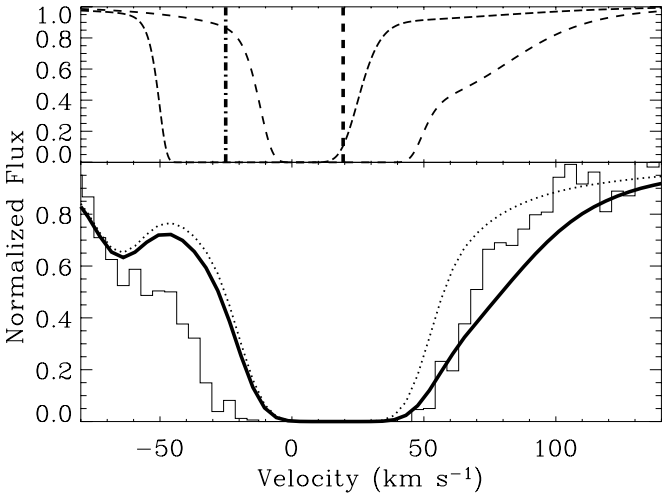

FIG. 2.—*Top*: Compares heliospheric H I Lyα absorption profiles plotted on a heliocentric velocity scale predicted for the upwind 36 Oph (*dot-dashed line*) and downwind Sirius (*dashed line*) lines of sight, based on a hydrodynamic model of the heliosphere (see text). The thick vertical lines indicate the projected ISM flow speed in these two directions. *Bottom*: *HST* spectrum of the Lyα absorption line observed toward Sirius (*histogram*). The dotted line is the ISM absorption alone for this line of sight. The broad absorption centered at +20 km s^{-1} is interstellar H I absorption and the weak absorption at about −65 km s^{-1} is from interstellar deuterium. The thick solid line is the predicted heliospheric absorption from the top panel (*dashed line*) combined with the ISM absorption.

2002). We will take a closer look at these downwind *HST* data to see if any evidence for heliosheath absorption can be found. If not, we will derive upper limits for the amount of absorption that can be present.

Finally, observed heliosheath absorption can potentially be used to constrain the flux of energetic neutral atoms (ENAs) that should be observable within our solar system. Local ENA fluxes should be dominated by neutrals created by charge exchange within the heliosheath that are then directed through the termination shock toward the Sun. Thus, locally observed ENAs basically sample the same particle population as the heliosheath absorption. In 2008, the *Interstellar Boundary Explorer* (*IBEX*), which is entirely devoted to studying ENAs, will be launched (McComas et al. 2005). Constraints on ENA fluxes from Lyα absorption will be valuable in preparation for this mission. Furthermore, the ASPERA-3 instrument on board the *Mars Express* satellite has already reported a detection of heliospheric ENAs (Galli et al. 2006). We will make an initial assessment as to whether the ENA fluxes observed by ASPERA-3 are consistent with heliosheath absorption detections and/or upper limits.

2. SEARCHING FOR EVIDENCE OF HELIOSHEATH ABSORPTION

2.1. *A Sirius Example of Heliosheath Absorption*

Currently, the only detection of heliospheric Lyα absorption in a downwind direction, where heliosheath absorption should dominate the hydrogen wall absorption, is for the Sirius line of sight at $\theta = 139°$. The Sirius data are shown in Figure 2. The ISM Lyα absorption for this line of sight is derived with the assistance of constraints provided by other ISM absorption lines (Bertin et al. 1995b). There is excess absorption on both sides of the Lyα line that cannot be accounted for by the ISM. The excess on the blue side of the line (at <-10 km s^{-1} in the figure) is believed to be from the stellar wind of Sirius, which is a hot A0 V star (Bertin et al. 1995a; Hébrard et al. 1999). The excess on the red side of the line (at >40 km s^{-1}), based on the ISM parameters derived by Bertin et al. (1995b), is claimed by Izmodenov et al. (1999) to be heliospheric absorption.

There are serious problems with this Sirius data, and with the detection of heliospheric absorption. The spectral resolution is lower than any other spectrum with a claimed heliospheric absorption detection. Thus, the wavelength calibration will be more uncertain. The signal-to-noise ratio (S/N) of the data is also low, as Figure 2 clearly shows. The presence of the wind absorption complicates the analysis of the blue side of the line, including the D I absorption (Hébrard et al. 1999). Finally, observations of narrower ISM lines demonstrate that there are actually two distinct ISM velocity components for this line of sight, which further complicates the Lyα analysis. Hébrard et al. (1999) are able to fit *HST* Lyα spectra of both Sirius and its companion Sirius B without any need for the existence of excess red-side absorption, but this interpretation of the data ideally requires the assumption of a very low D/H ratio for the weaker of the two ISM components seen toward Sirius, which would contradict recent claims that D/H within the Local Bubble is constant, with a value around D/H $\approx 1.5 \times 10^{-5}$ (Linsky 1998; Moos et al. 2002; Wood et al. 2004). Thus, we still consider the presence of excess red-side absorption, possibly heliospheric in origin, to be a plausible interpretation of the data. Despite its problems, the line of sight does have the advantage of having one of the lowest ISM H I column densities ever observed, due mostly to its very short distance of $d = 2.6$ pc. The Bertin et al. (1995b) analysis suggests an ISM column density (in cm^{-2}) of $\log N_{\rm H} = 17.53$, while Hébrard et al. (1999) infer $\log N_{\rm H} = 17.81$. Both values are lower than any other *HST*-observed downwind line of sight. With the ISM absorption being therefore weaker than any other downwind line of sight, this would explain why Sirius is so far the only such line of sight with a heliospheric absorption detection.

Figure 2 also shows the absorption predicted by a hydrodynamic model of the heliosphere. The model used here is of the type described by Baranov & Malama (1993, 1995), which includes

a fully kinetic treatment of the neutrals within the heliosphere. The neutral hydrogen density, proton density, velocity, and temperature of the undisturbed ISM assumed in this model are $n_\infty(\mathrm{H\ I}) = 0.18\ \mathrm{cm}^{-3}$, $n_\infty(\mathrm{H}^+) = 0.06\ \mathrm{cm}^{-3}$, $V_\infty = 26.4\ \mathrm{km\ s}^{-1}$, and $T_\infty = 6400$ K. The top panel of Figure 2 shows absorption predicted for both the upwind 36 Oph line of sight (at $\theta = 12^\circ$) and the downwind Sirius line of sight ($\theta = 139^\circ$). We choose the 36 Oph line of sight for comparison because it represents the most upwind detection of heliospheric absorption, while Sirius is the only downwind detection (Wood et al. 2005b). Both absorption profiles are significantly redshifted relative to the local ISM flow speed in those directions, based on the Local Interstellar Cloud vector (Lallement & Bertin 1992; Lallement et al. 1995). This is why heliospheric absorption is always found on the red side of the ISM absorption. Since astrospheric absorption is observed from outside the astrosphere rather than inside, it is conversely found on the *blue* side of the ISM absorption.

The absorption predicted for the Sirius line of sight is added to the ISM absorption and the result is compared with the data in Figure 2. The model appears to predict too much absorption at $>60\ \mathrm{km\ s}^{-1}$. Similar results have previously been found when comparing other kinetic models with downwind observations (Wood et al. 2000; Izmodenov et al. 2002). Since charge exchange processes drive the neutrals in the heliosphere out of thermal equilibrium, models with a fully kinetic treatment of the neutrals would seem to be necessary to provide the most precise description of neutral velocity distributions within the heliosphere, which in turn should provide the most accurate Lyα absorption profiles. Nevertheless, these kinetic models generally seem to overpredict heliosheath absorption in downwind directions.

However, the nature of the heliosheath absorption predicted by the models is such that it is not easy to entirely rule out its presence for observed downwind lines of sight. The top panel of Figure 2 shows that the heliosheath absorption toward Sirius is characterized by a very broad, extended wing on the red side of the profile. This is very different from the absorption profile for the upwind 36 Oph line of sight, which is dominated by the hydrogen wall. Heliosheath neutrals are generally much hotter than hydrogen wall neutrals, but heliosheath neutral column densities are much lower. This is why the heliosheath absorption tends to be broad but shallow compared to the hydrogen wall absorption. Note that there is a weak extended wing for the 36 Oph absorption that would correspond to heliosheath absorption in that direction, but the absorption is too weak to be detectable. The weakness of the wing is simply because the heliosheath is much narrower in upwind directions (see Fig. 1). The hydrogen wall absorption produces a rather sharp, well-defined absorption edge, which is something that can be compared with the data in a reasonably definitive manner to see whether the model is consistent with the data. However, the broad extended wing of the heliosheath absorption in downwind directions complicates matters, for reasons we now describe.

One of the primary sources of systematic uncertainty in any of these Lyα analyses is the reconstruction of the background stellar Lyα profile (Wood et al. 2005b). No reasonable change to an assumed stellar profile will greatly change the velocity where the Lyα absorption predicted by a model becomes saturated. This is why the sharp absorption edge provided by the hydrogen wall absorption provides a much better diagnostic to compare with the data than the broad absorption wing that characterizes the heliosheath absorption, which results in the apparent disagreement with the data in Figure 2. The red-wing absorption discrepancy in Figure 2 could in principle be resolved by increasing by $\sim$30% the background Sirius Lyα fluxes from 60 to 120 km s^{-1}. Other examples of how stellar Lyα profiles can be modified to allow such broad wing absorption are presented by Wood et al. (2000) and Izmodenov et al. (2002). There is still a limit, however, to how much one can modify the stellar profile in this fashion before the resulting profile becomes implausible, and there is therefore a limit to how much extended wing absorption can be present. For example, modifying the Sirius Lyα background as described above would create a dubious asymmetry in the stellar Lyα absorption profile. Quantifying exactly when "dubious" becomes "completely unreasonable" is not easy, but that is the task that we now undertake.

2.2. *Stellar Lyα Line Bisector Analysis*

Most *HST*-observed nearby stars that are appropriate targets to search for heliospheric and/or astrospheric absorption are cool main sequence stars like the Sun (Wood et al. 2005b). The Lyα lines of such stars are relatively narrow, isolated emission lines. Note that Sirius is a hot A0 V star whose stellar profile is instead a very broad absorption line, so Sirius is unfortunately not a representative example at all. As shown in Figure 2, heliosheath absorption will contaminate only the red side of a stellar emission line. Therefore, if there is unrecognized and undetected heliosheath absorption, the stellar Lyα emission profile reconstructed from the *HST* data will end up blueshifted with respect to the stellar rest frame.

The wings of the Lyα line will be formed in the chromosphere of the observed star. Although emission lines formed at higher temperatures in the transition region can be shifted from the stellar rest frame, the wings of Lyα should be centered on the star (Ayres et al. 1988; Wood et al. 1997). We can search for previously undetected absorption from the heliosheath by searching for cases in which reconstructed Lyα profiles end up blueshifted with respect to the star. The requirement that a stellar emission line be centered on the stellar radial velocity also provides a way to limit modifications to the stellar profile, thereby yielding upper limits to the amount of broad heliosheath absorption that can be present in the red wing of the Lyα line.

Wood et al. (2005b) provide a complete list of *HST* Lyα spectra of nearby stars, all 62 of which have been analyzed to measure ISM H I and D I column densities, search for heliospheric/astrospheric absorption, measure chromospheric Lyα line fluxes corrected for ISM absorption, etc. From this list we choose a selection of stars to look for shifts in the reconstructed Lyα line relative to the stellar radial velocity. We exclude hot stars, which have Lyα in absorption rather than emission. We exclude giant stars, which have Lyα emission lines that are too broad to be effective for our purposes. We also exclude short-period, unresolved binaries, partly because the stellar rest frame can change due to orbital motion during the course of the observation, and partly because in some cases both stars contribute to the Lyα emission, meaning there is no single stellar rest frame. We only consider data with reasonably high S/N, and with a spectral resolution of at least $\lambda/\Delta\lambda = 40{,}000$ to maximize our confidence in the wavelength calibration.

And finally, we only consider lines of sight with ISM column densities of $\log N(\mathrm{H\ I}) < 18.3$. High-ISM columns potentially degrade the effectiveness of our analysis in a couple of ways. Broad ISM absorption limits us to the far wings of the Lyα profile in our search for Lyα line shifts. Also, the damping wings of the ISM Lyα absorption are much stronger at higher columns, and when the absorption is not exactly centered on the rest frame of the star, uncertainties in the ISM H I column density can potentially lead to a shift in the reconstructed stellar Lyα line that could mimic the shifts we are looking for due to heliosheath absorption.

TABLE 1
Lyα Line Velocities

Star	θ (deg)	V_{bis} (km s^{-1})	V_{rad} (km s^{-1})	References
36 Oph A	12.3	0.2	0.5 ± 0.2	1
70 Oph A	23.8	−6.8	−7.9 ± 0.5	2
HD 165185	25.4	13.5	14.9 ± 0.1	3
HD 128987	33.3	−22.8	−23.0 ± 0.1	3
ξ Boo A	46.2	0.2	1.3 ± 0.1	4
α Cen B	52.4	−20.7	−20.8 ± 0.5	5
61 Vir	53.1	−7.5	−7.9 ± 0.1	4
χ Her	59.6	−54.1	−56.1 ± 0.1	4
ϵ Ind	69.8	−38.9	−38.9 ± 0.3	6
61 Cyg A	78.3	−65.3	−65.7 ± 0.1	4
HD 116956	84.4	−12.8	−12.3 ± 0.1	3
HD 97334	96.6	−2.0	−3.7 ± 0.1	4
EV Lac	98.2	3.0	0.4 ± 0.1	4
ζ Dor	107.7	−1.4	−0.7 ± 0.1	7
HD 166	111.0	−7.5	−6.5 ± 0.1	4
DK UMa	111.5	−27.6	−27.3 ± 0.1	8
β Cas	111.8	13.3	11.3 ± 0.5	9
HD 73350	122.1	33.8	35.4 ± 0.1	4
τ Cet	122.9	−18.2	−16.6 ± 0.1	4
HD 43162	137.3	22.1	21.7 ± 0.1	3
HD 37394	140.3	1.1	1.2 ± 0.1	4
ϵ Eri	147.4	17.9	16.3 ± 0.1	4
δ Eri	148.8	−8.8	−6.3 ± 0.1	4
κ Cet	152.5	16.4	19.0 ± 0.1	4
40 Eri A	154.7	−42.4	−42.3 ± 0.1	4
χ^1 Ori	166.3	−21.1	−15.3 ± 0.5	10, 11
HD 28205	172.0	33.2	39.3 ± 0.2	12
HD 28568	173.3	30.3	40.9 ± 1.3	12

References.—(1) Beavers & Eitter 1986; (2) Tokovinin & Smekhov 2002; (3) Gaidos et al. 2000; (4) Nidever et al. 2002; (5) Pourbaix et al. 2002; (6) Buscombe & Kennedy 1968; (7) Murdoch et al. 1993; (8) Duquennoy et al. 1991; (9) Duflot et al. 1995; (10) Gullberg & Lindegren 2002; (11) Irwin et al. 1992; (12) Perryman et al. 1998.

Our selection criteria reduce the original sample of Lyα spectra to 28 targets. These are listed in Table 1 in order of increasing θ. Our analysis requires accurate knowledge of the stellar photospheric radial velocity, V_{rad}. The fourth column of Table 1 lists V_{rad} for all of our stars, and the last column provides the references for these values. The quoted uncertainties are generally from these references, but we set a floor of 0.1 km s^{-1} for the uncertainties in Table 1. For cases in which the observed star is a member of a binary system (particularly α Cen B and χ^1 Ori), we have to consider the effects of orbital motion to establish the precise radial velocity at the time of observation, so we have increased the quoted uncertainty accordingly.

Figure 3 illustrates how we measure the velocities of the stellar Lyα lines, using eight of the stars in Table 1 as examples. The figure shows the observed Lyα spectra and the reconstructed stellar line profiles. We refer the reader to Wood et al. (2005b and references therein) for details on the reconstruction process, and for complete illustrations of the line profiles. We note that all the stellar profiles used here yield D/H values consistent with the D/H = $(1.56 \pm 0.04) \times 10^{-5}$ value now believed to apply throughout the Local Bubble (Wood et al. 2004). Many of the analyses actually *assumed* this value (e.g., Wood et al. 2005b), in which case the H I column density is directly inferred from the more easily measured D I column. Since the wings of the H I absorption depend solely on the H I column density and not on the Doppler parameter, the wings of the stellar Lyα profile can then be inferred simply by computing the Lyα opacity profile, τ_λ, from the H I column density and multiplying the observed wings by $\exp \tau_\lambda$.

In Figure 3, we focus only on the lower flux part of the Lyα profile, where we can measure meaningful line centroids for comparison with the radial velocity. The top parts of the profile are not useful for our purposes for two reasons. The first is that the section of the profile above the saturated core of the ISM H I absorption is in reality completely unconstrained by the data. The second is that cool star Lyα line profiles (including that of the Sun) can have asymmetric self-reversals near line center (see Wood et al. 2005b), meaning that this part of the profile will not necessarily be centered on the star.

The horizontal dotted lines in Figure 3 indicate flux levels at which we measure the centroid of the line. Collectively, these centroids form a line bisector. These bisectors are shown as near-vertical solid lines in the figure. For five of the stars (70 Oph A, ϵ Ind, ζ Dor, τ Cet, and ϵ Eri) the bisector ends up where we expect it, very close to the stellar radial velocity. However, for the three most downwind lines of sight (χ^1 Ori, HD 28205, and HD 28568) the bisector is significantly blueshifted with respect to the star. This is exactly the signature of undetected heliosheath absorption that we are looking for, and the downwind direction is where we expect to see it.

We compute the average velocity of the bisector, V_{bis}, for each star, ignoring the lowest two flux levels, where low S/N in the extreme far wings of the line sometimes causes unreasonable excursions in the bisector (e.g., HD 28568 in Fig. 3). These bisector velocities are listed in Table 1. We define the discrepancy between these velocities and the stellar rest frame as $\Delta V \equiv V_{bis} - V_{rad}$. In Figure 4, ΔV is plotted against θ for all the stars listed in Table 1.

For the three $\theta > 160^\circ$ cases, the Lyα profile is significantly blueshifted. This blueshift is common to all $\theta > 160^\circ$ lines of sight, is not seen in other directions, and is exactly in the direction where we would expect heliosheath absorption to be maximized. Thus, we conclude that it is highly likely that heliosheath absorption is responsible for these Lyα blueshifts. For each of these stars, we can construct a stellar profile that is forced to be centered on the stellar rest frame by reflecting the blue wing of the original reconstructed profile across the stellar radial velocity onto the red wing. The flux difference between the red wing of this profile and the original one provides an estimate of the heliosheath absorption that is present, which can be compared with the predictions of hydrodynamic models of the heliosphere.

Other than the three $\theta > 160^\circ$ sight lines, the reconstructed Lyα profiles are encouragingly close to their expected locations at the stellar radial velocity. The average and standard deviation of the $\theta < 160^\circ$ data points is $\Delta V = 0.0 \pm 1.4$ km s^{-1}. The scatter can be easily explained by uncertainties in the spectral wavelength calibration and systematic errors present in the profile reconstruction process. We note that most of the *HST* data for the stars listed in Table 1 are STIS E140M spectra, which have demonstrated 1 σ random wavelength calibration uncertainties of ± 0.9 km s^{-1} (Wood et al. 2005b). This same analysis also found a systematic offset of -1.2 km s^{-1} for STIS E140M Lyα spectra. We corrected all the STIS E140M spectra for this shift before starting the bisector analysis. The centering of the ΔV values on 0 km s^{-1} (for $\theta < 160^\circ$) implies that this correction successfully removed all significant systematic wavelength calibration problems.

None of the $\theta < 160^\circ$ profiles is shifted away from the stellar rest frame by more than 3 km s^{-1}. These results imply that a reconstructed stellar Lyα line should be within 3 km s^{-1} of the stellar rest frame to be reasonable. This limits how much the Lyα profiles can be changed to allow for potential heliosheath

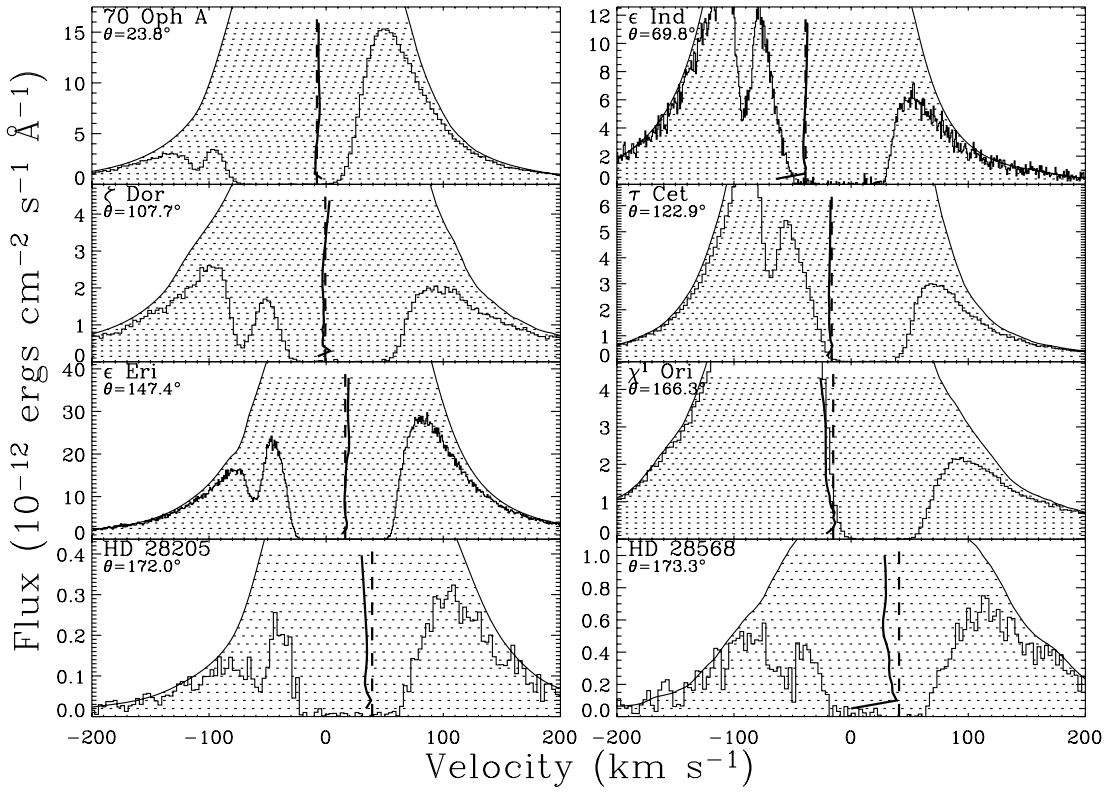

FIG. 3.—Lyα line bisector measurements for various stars. The histograms are the *HST* Lyα spectra. The broad absorption dominating the observed line profiles is H I absorption, and the weak absorption about -82 km s^{-1} from the center of the H I absorption is from interstellar deuterium. The solid lines above the data are the reconstructed stellar Lyα profiles. The dotted lines indicate the flux levels at which the bisectors of the stellar profiles are measured, which are the thick near-vertical solid lines. The vertical dashed lines are the stellar radial velocities. Note that for the three most downwind lines of sight (χ^1 Ori, HD 28205, and HD 28568) the bisector is blueshifted relative to the stellar rest frame, suggesting the presence of heliosheath absorption in the red wing of the line.

absorption. We can therefore use these limits to establish upper bounds on the amount of heliosheath absorption that can be present for the $\theta < 160^\circ$ lines of sight listed in Table 1.

To construct an upper limit to the red wing of the Lyα profile, we define an upper limit bisector that at all flux levels is +3 km s^{-1} from the stellar radial velocity or +3 km s^{-1} from the velocity of the original bisector, whichever is largest. An upper limit for the red wing of the Lyα profile is then derived by reflecting the blue wing of the original reconstructed profile across the upper limit bisector. Figure 5 shows the result for the case of τ Cet. The difference between the upper limit profile and the original one represents an estimate of the maximum amount of heliosheath absorption that can be present in that direction.

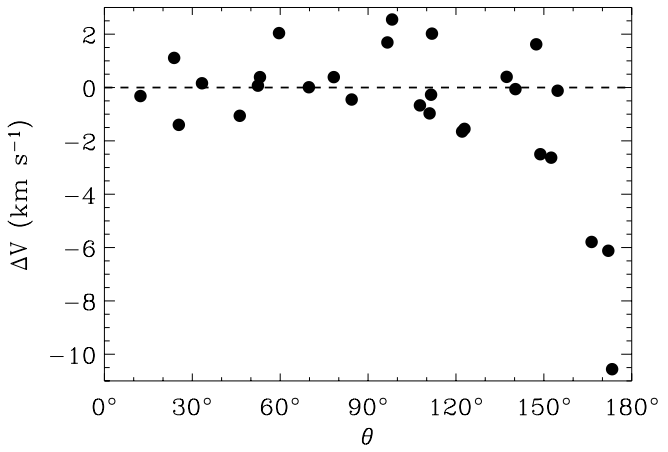

FIG. 4.—Velocity differences between the Lyα line bisector and the stellar rest frame ($\Delta V \equiv V_{\rm bis} - V_{\rm rad}$) plotted as a function of θ, the line-of-sight orientation with respect to the ISM flow vector. There is evidence that Lyα profiles reconstructed for the most downwind lines of sight ($\theta > 160^\circ$) are systematically blueshifted with respect to the stellar rest frame, suggesting the presence of heliosheath absorption.

One final issue worthy of mention concerns astrospheric absorption. If we observed a star through the downwind tail of its astrosphere, it is possible that astrosheath absorption would lead to a reconstructed stellar Lyα profile that is *redshifted* relative to the star rather than blueshifted, keeping in mind that astrospheric absorption appears on the opposite side of the Lyα line from the heliospheric absorption (see § 2.1). However, Figure 4 shows no data points with $\Delta V > +3$ km s^{-1}. Given that a heliospheric effect is only seen for $\theta > 160^\circ$, we conclude that either none of these 28 sight lines has $\theta > 160^\circ$ for the stellar astrosphere, or if there are any $\theta > 160^\circ$ astrospheric lines of sight, the ISM surrounding the star contains no neutrals to provide Lyα absorption, which should be a common occurrence within the mostly ionized Local Bubble (Wood et al. 2005b).

3. MODELS WITH SINGLE- AND MULTI-COMPONENT PLASMAS

As an example of how the heliosheath absorption detections and upper limits can be used, we now compare the Lyα data with the predictions of a pair of heliospheric models. One of the models is the kinetic model described in § 2.1 and used in Figure 2. This model is of the Baranov & Malama (1993, 1995) type, which uses a fully kinetic treatment of the neutrals but treats the plasma as a single hydrodynamic fluid. This plasma treatment is simplistic. The best evidence for this concerns pickup ions inside

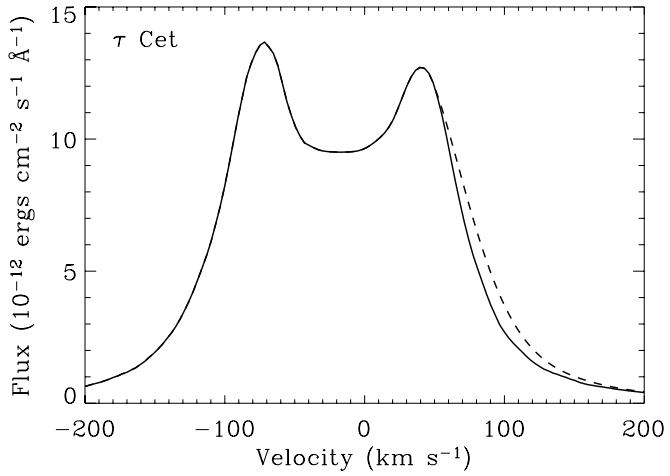

FIG. 5.—Reconstructed stellar Lyα profile for τ Cet (*solid line*), and an upper limit for the red wing of the profile (*dashed line*) derived by requiring that the profile be within 3 km s^{-1} of the stellar radial velocity (see text).

the termination shock (region 1 in Fig. 1). Pickup ions originate from charge exchange between outflowing solar wind protons and inflowing ISM neutrals, which creates a solar wind neutral H atom and an inflowing ion that is then "picked up" by the solar wind. Observations show that the pickup ions are not thermalized with the solar wind, and the pickup ions also show non-Maxwellian velocity distributions (e.g., Gloeckler & Geiss 2004). Thus, combining solar wind plasma and pickup ions into a single fluid in a heliospheric model, as is typically done, will lead to inaccuracies in the particle distributions.

Malama et al. (2006) have recently attempted to solve this problem by modifying the Baranov & Malama heliospheric modeling code to allow a complex multicomponent treatment of the plasma, as well as including the usual full kinetic treatment of the neutrals. We consider here a multicomponent model of this type using the same input parameters assumed in the single-component model (see § 2.1). Figure 1 shows the differences in global heliospheric structure suggested by the two models.

Figure 6 compares the absorption predicted by the single- and multicomponent models with the Lyα absorption observed for four downwind lines of sight, including the Sirius line of sight discussed in § 2.1. The figure focuses on the red side of the absorption, where the heliospheric absorption should be located. Using the original reconstructed stellar profiles, the ISM absorption alone is illustrated, and the absorption predicted by the heliospheric models is shown after being added to the ISM absorption.

Dashed lines in Figure 6 indicate the extra heliosheath absorption that is allowable by the data based on the upper limit stellar profiles derived as described in the previous section (see Fig. 5). Models can be considered to be consistent with the data if they do not predict more absorption than these dashed lines, so the dot-dashed lines should lie above the dashed lines in Figure 6. The dashed lines have a lower velocity limit in Figure 6. This is because the line bisector analysis described above is not applicable close to line center (for reasons discussed in § 2.2), so we cannot really quantify an upper limit to the profile near line center. No absorption limits have been derived for Sirius, since it is a hot star

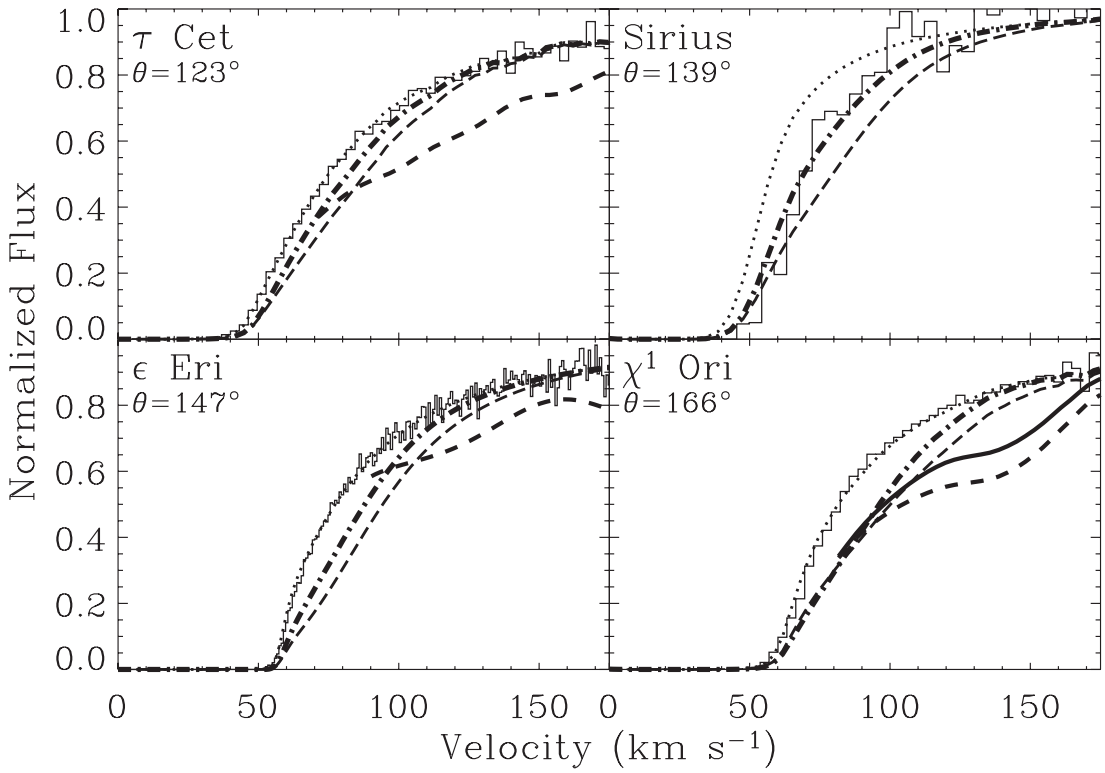

FIG. 6.—Normalized Lyα spectra in downwind directions, focusing on the red side of the Lyα absorption line where the heliospheric absorption resides. The dotted line is the ISM absorption alone, which can account for all the observed absorption, except for Sirius. The thin and thick dot-dashed lines are the predicted heliospheric Lyα absorption of models with a single plasma fluid component and a multicomponent plasma treatment, respectively (see text). The dashed lines (when present) are the maximum heliospheric absorption that is allowable by the data, based on upper limit stellar Lyα profiles derived as described in the text. The models can be considered consistent with the data if their predicted absorption lies above these dashed lines. For χ^1 Ori, there is evidence from a blueshift of the original reconstructed Lyα line that there is extended heliosheath absorption present, and the thick solid line is the amount of absorption that should be observed if the real stellar Lyα line is centered on the stellar rest frame.

whose stellar profile is a broad absorption line rather than a comparatively narrow emission line (see § 2.2). However, as described in § 2.1, this is the one downwind line of sight with a previous detection of heliosheath absorption, with the ISM absorption underpredicting the observed absorption in Figures 2 and 6.

As described in § 2.2, the Lyα bisector analysis suggests that χ^1 Ori and two other very downwind lines of sight (HD 28205, HD 28568) show evidence for broad heliosheath absorption. The thick solid line in the χ^1 Ori panel of Figure 6 corresponds to the amount of excess absorption that *should* be present to allow a stellar line profile that is centered on the rest frame of the star. For χ^1 Ori, therefore, the model absorption in Figure 6 is best compared with the thick solid line rather than with the data. We could have added panels for HD 28205 and HD 28568 to Figure 6, but this would be somewhat redundant since the χ^1 Ori, HD 28205, and HD 28568 lines of sight are very similar, and the χ^1 Ori data are in any case far superior to the others in terms of S/N. The negative radial velocity of χ^1 Ori profile also makes that line of sight superior to HD 28205 and HD 28568. A blueshifted profile means that the bisector method can detect and quantify heliosheath absorption at lower heliocentric velocities than for redshifted profiles like those of HD 28205 and HD 28568, since you cannot do the search close to the center of the stellar profile. For χ^1 Ori, we can extend the dashed and solid lines down to $\sim$80 km s^{-1} (see Fig. 6), but for HD 28205 and HD 28568 this could only be done down to $\sim$130 km s^{-1}.

The absorption limits (Fig. 6, *dashed lines*) allow a significant amount of broad heliosheath absorption to exist while still being consistent with the data. Thus, the initial impression of disagreement between the models and the data in Figures 2 and 6 is partly illusory. The multicomponent model predicts less absorption than the single-component model. This provides better agreement with the data, particularly for the Sirius line of sight. The absorption predicted by the single-component model may be in conflict with the absorption limit toward ϵ Eri near 100 km s^{-1}, but the conflict is greatly lessened for the multicomponent model. The greater amount of broad heliosheath absorption for the single-component model indicates that the simplistic treatment of the plasma in this model overemphasizes the effects of minority high-temperature constituents on the plasma velocity distribution. The effect is to artificially broaden the distribution, a problem that is then transmitted to the neutral distributions via charge exchange.

One very important caveat that must be mentioned is that the heliospheric models that we have employed here use a spatial grid that extends only 700 AU from the Sun (see Fig. 1), which may not extend far enough to capture all the heliospheric absorption in downwind directions along the lengthy tail of the heliosphere. Thus, the model absorption predictions in Figure 6 may end up being lower limits to the actual amount of absorption that these models would really predict given a sufficiently large grid. This problem could potentially worsen agreement between the models and the data, particularly for the most downwind directions where the bisector analysis has provided new evidence for heliosheath absorption. In the future, we will expand the grid for the multicomponent model up to 10,000 AU, as has already been done for single-fluid Baranov & Malama models (Izmodenov & Alexashov 2003; Aleksashov et al. 2004).

4. CONNECTING HELIOSHEATH ABSORPTION WITH LOCAL ENA FLUXES

The ASPERA-3 instrument on *Mars Express* was designed primarily to study particles escaping from the Martian atmosphere (Barabash & Lundin 2006). However, ASPERA-3 has detected ENAs even when not pointed at Mars, both en route to Mars and while in orbit around the planet. Galli et al. (2006) and Wurz et al. (2006) have argued that a heliosheath origin for these particles is more likely than a more local interplanetary source.

The particle energy spectra observed for the nonplanetary ENAs are nearly always consistent with the following power-law behavior (Galli et al. 2006):

$$f(E) \propto \begin{cases} E^{-1.6}, & E < 0.77 \text{ keV}, \\ E^{-3.3}, & E \geq 0.77 \text{ keV}. \end{cases} \quad (1)$$

Particle fluxes are variable, although the nature of the ASPERA-3 observations makes it difficult to distinguish temporal from spatial variability. Within ASPERA-3's energy range of 0.2–10 keV, logarithmic particle fluxes are in the range $\log F_{\rm A3} = 3.7$–5.0 (in units of cm^{-2} s^{-1} sr^{-1}). If the nonplanetary ENAs observed by ASPERA-3 are indeed heliosheath neutrals, they then represent the same particle population that we have been investigating with regards to the Lyα absorption produced by these neutrals. Thus, we can in principle test the heliosheath interpretation of the nonplanetary ASPERA-3 ENAs by seeing if the observed fluxes are consistent with the Lyα data.

Dotted lines in Figure 7 illustrate the observed energy spectrum given by equation (1), with the lower and upper lines indicating the lower and upper range of observed fluxes, respectively. The lower bound of ASPERA-3's energy range, 0.2 keV, represents a particle velocity of 196 km s^{-1}. This corresponds with the *upper* bound of the 50–200 km s^{-1} velocity range, within which the Lyα data provide the best absorption constraints (see Fig. 6). Thus, before we can even hope to use the ASPERA-3 measurements to predict Lyα absorption, we must extrapolate the ASPERA-3 energy spectra to lower energies. There are three different extrapolations assumed in Figure 7. The solid line simply continues the $E^{-1.6}$ power law to lower energies. The dashed line assumes a flat spectrum below 0.2 keV, and the dot-dashed line assumes a drop in flux below 0.2 keV. The four Figure 7 panels show the resulting spectra for four different values of $\log F_{\rm A3}$.

The biggest difficulty in connecting the ASPERA-3 ENA and *HST* Lyα data lies in the issue of how to extrapolate a locally observed particle spectrum along an entire line of sight through the heliosphere. If the heliosheath is the source of the ENAs, then for our purposes the region inside the termination shock (region 1 in Fig. 1) is in effect an empty cavity that is being filled by a flux of heliosheath particles from all directions. The heliosphere is not spherically symmetric, so it is likely that fluxes will be larger from some directions than others. Nevertheless, assuming that within the termination shock the particle distributions are isotropic and the same throughout region 1 may be a reasonable first-order approximation. This will probably not be the case within the heliosheath itself. Thus, for our purposes here, we will confine our attention only to absorption by heliosheath neutrals within the termination shock.

In downwind directions, which are the most appropriate for heliosheath Lyα absorption, the termination shock distance is about 200 AU (see Fig. 1). The inset figures in Figure 7 show the Lyα absorption produced by heliosheath neutrals within this distance, assuming that the ENA spectra shown in the figure are isotropic and apply along the entire 200 AU path length. The absorption limits derived for the τ Cet and ϵ Eri lines of sight in § 2.2 (see Fig. 6) are also shown, for comparison with the absorption predicted by the ENA spectra.

The two highest flux values explored in Figure 7, $\log F_{\rm A3} = 4.55$ and $\log F_{\rm A3} = 4.95$, clearly lead to too much Lyα absorption to be consistent with the limits from the *HST* data. A flux of $\log F_{\rm A3} = 4.15$ is only consistent with the Lyα data if fluxes

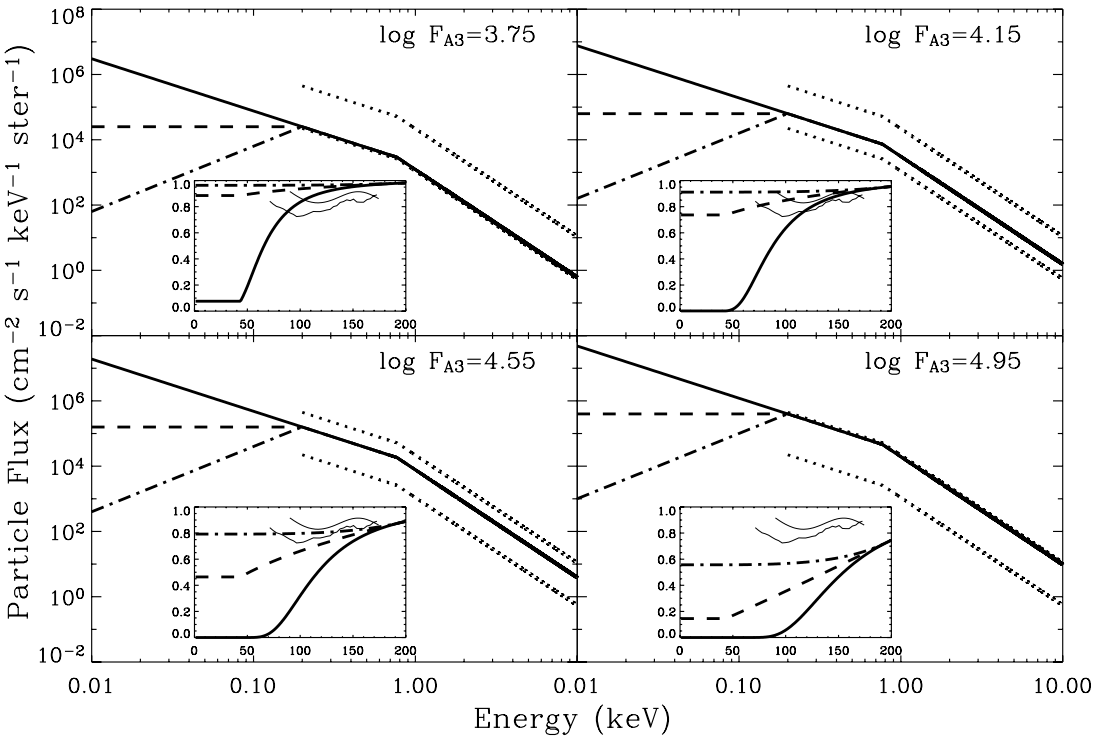

FIG. 7.—Dotted lines in each panel encompass the range of ENA spectra observed by ASPERA-3, corresponding to different 0.2–10 keV particle fluxes (in units of cm^{-2} s^{-1} sr^{-1}) of $\log F_{A3} = 3.7$–5.0. Assuming different fluxes within this range, each panel shows three different spectra, which use different extrapolations to low energies. The inset panels show the H I Lyα absorption from within the termination shock predicted by these spectra, plotted on a heliocentric velocity scale (in km s^{-1}). The two thin solid lines that stretch from $\sim$70 to 175 km s^{-1} are the absorption limits derived for τ Cet and ϵ Eri based on the Lyα bisector analysis (see § 2.2 and Fig. 6). The absorption predicted by the energy spectra must lie above these limits to be consistent with the Lyα data.

decrease below 0.2 keV, and even the lowest flux of $\log F_{A3} = 3.75$ is only consistent with the absorption limits if the particle fluxes are flat or decrease below 0.2 keV. The situation is actually even worse than this, given that the absorption predictions in Figure 7 only include absorption from within the termination shock. Considering that a downwind line of sight will have a path length through the heliosheath much longer than the $\sim$200 AU path length inside the termination shock, it is clear that including absorption from the heliosheath could easily increase the amount of absorption many times above the predictions shown in Figure 7. With this in mind, it is very questionable whether *any* of the energy spectra in Figure 7 are consistent with the relative lack of heliospheric absorption observed in downwind directions. At the very least, the spectrum must lie near the lower bound of the ASPERA-3 range, with fluxes that decrease to lower energies. It is worth noting that the flux range quoted by Galli et al. (2006) does not take into account numerous upper limits when no ENAs were detected (see Fig. 4 in Galli et al. 2006), suggesting that perhaps the lower bound could be decreased further without being truly discrepant with the ASPERA-3 data.

Nevertheless, our difficulty in reconciling the ASPERA-3 ENA fluxes with the *HST* Lyα spectra is a strong argument against the ASPERA-3 ENAs being heliosheath neutrals. Galli et al. (2006) acknowledge other difficulties with the heliosheath interpretation. One is that many heliospheric models predict ENA fluxes at Earth about an order of magnitude lower than those observed by ASPERA-3 (Gruntman et al. 2001; Wurz et al. 2006). The substantial variability seen by ASPERA-3 is also potentially difficult for a distant heliosheath source to explain, and is more suggestive of a local interplanetary source. Identifying the origin of the ASPERA-3 ENAs is particularly important considering the upcoming 2008 launch of *IBEX*, which unlike ASPERA-3 is entirely designed and devoted to studying heliosheath ENAs. If there is an unexpectedly strong local interplanetary ENA source that is responsible for the ASPERA-3 ENAs, *IBEX* will presumably see it as well and will somehow have to distinguish between these particles and the true heliosheath ENAs to accomplish its mission. It is also worth noting that the ASPERA-4 instrument on board *Venus Express* will soon be able to confirm or refute ASPERA-3's measurements of nonplanetary ENAs.

Based on Figure 7, we quote a very conservative upper limit of $F < 5000$ cm^{-2} s^{-1} sr^{-1} for the local flux of heliosheath ENAs in the 0.01–0.2 keV energy range most applicable to the Lyα absorption data. The ASPERA-3 and ASPERA-4 instruments are not sensitive to these low energies, but *IBEX* will be. Unless the heliosheath unexpectedly produces significantly less absorption than the region inside the termination shock, the actual 0.01–0.2 keV flux can be expected to be well below this limit. More precise constraints on ENA fluxes from the Lyα data will require the assistance of kinetic heliospheric models to better connect heliosheath absorption along a downwind line of sight with the ENA energy spectrum close to the Sun. Once *IBEX* is launched it will be very interesting to see if heliospheric models are capable of simultaneously reproducing both the local ENA spectrum and the heliosheath absorption data, particularly the previously detected absorption toward Sirius and the three new $\theta > 160^\circ$ detections reported here for the first time.

5. SUMMARY

The absorption within the Lyα lines of nearby stars sometimes has a detectable heliospheric contribution, in addition to the ubiquitous interstellar H I and D I absorption. Most detections are in upwind directions, where the hydrogen wall dominates the absorption. However, in this paper we have focused

on absorption from the heliosheath, which is only prominent in downwind directions. Our findings are as follows:

1. In order to search for evidence of previously undetected heliosheath absorption, we have measured the bisectors of 28 stellar Lyα lines reconstructed from the data after correcting for the broad ISM absorption (and heliospheric/astrospheric absorption, when present). We find that the stellar Lyα profiles of the three most downwind lines of sight (χ^1 Ori, HD 28205, and HD 28568), all with $\theta > 160^\circ$, are significantly blueshifted relative to the stellar radial velocities. This is indicative of broad absorption in the red wing of the Lyα line that was not accounted for in the reconstruction of the stellar profile. This is exactly the signature of heliosheath absorption we are looking for, and the most downwind lines of sight are where we expect to see it. Thus, we add these three lines of sight to the list of eight previous heliospheric Lyα absorption detections, only one of which (Sirius) is a downwind line of sight. For the three new detections, the amount of heliospheric absorption can be estimated by reanalyzing the Lyα data using a stellar profile that is forced to be centered on the stellar rest frame.

2. The stellar Lyα profiles of the 25 lines of sight with $\theta < 160^\circ$ are all found to be within ± 3 km s^{-1} of the stellar radial velocity. This represents a conservative quantitative estimate of the accuracy of the reconstructed Lyα profiles. We can define an upper limit to the red wing of the stellar Lyα profile by requiring the bisector to be no more than +3 km s^{-1} from either the stellar radial velocity or the bisector of the original reconstructed profile, whichever is greatest. In this way, we derive for the first time quantitative upper limits for the amount of broad heliosheath absorption that can be present in the red wings of Lyα lines without clearly detectable heliosheath absorption.

3. We compare the Lyα absorption predicted by two kinetic heliospheric models with downwind Lyα lines observed by *HST*. One model uses the complex multicomponent plasma treatment discussed by Malama et al. (2006), while the other uses a simple single-fluid approach. The multicomponent model predicts significantly less heliosheath absorption than the single-fluid model, in better agreement with the data. This suggests that the single-fluid plasma approach, which is the usual assumption in heliospheric models, may not reproduce particle distribution functions accurately enough for some applications.

4. Meaningful comparisons between models and the Lyα absorption data in downwind directions require the use of a model grid that extends a sufficiently long distance down the tail of the heliosphere to capture all of the heliosheath absorption. Most hydrodynamic models of the heliosphere, including the ones used here, do not extend the grid far enough for these purposes. In the future, we hope to perform more precise data/model comparisons using sufficiently large grids.

5. The ASPERA-3 instrument on board *Mars Express* has detected a substantial flux of nonplanetary ENAs, which have been interpreted as being heliosheath neutrals. We believe that the observed ENA fluxes likely predict too much heliosheath Lyα absorption in downwind directions to be consistent with the *HST* Lyα spectra. This represents a strong argument against a heliosheath origin for these ENAs, instead suggesting a local interplanetary source.

6. The *HST* Lyα absorption data can provide useful constraints on the heliosheath ENA fluxes that *IBEX* can expect to observe when launched in 2008. We here quote a very conservative upper limit of $F < 5000$ cm^{-2} s^{-1} sr^{-1} for the local flux of heliosheath ENAs in the 0.01–0.2 keV energy range most applicable to the Lyα absorption data. We hope to compute more stringent constraints in the future using kinetic models of the heliosphere to connect particle distributions in the heliosheath with those that *IBEX* will observe locally.

We would like to thank Peter Wurz for providing information on the ASPERA-3 instrument and its measurements. This work was supported by NASA grant NNG05GD69G to the University of Colorado. V. I. was also supported by RFBR grant 04-02-16559, the Dynastia Foundation, and the Foundation in Support of Russian Science.

REFERENCES

Aleksashov, D. B., Izmodenov, V. V., & Grzedzielski, S. 2004, Adv. Space Res., 34, 109
Ayres, T. R., Jensen, E., & Engvold, O. 1988, ApJS, 66, 51
Barabash, S., & Lundin, R. 2006, Icarus, 182, 301
Baranov, V. B., Lebedev, M. G., & Malama, Y. G. 1991, ApJ, 375, 347
Baranov, V. B., & Malama, Y. G. 1993, J. Geophys. Res., 98, 15157
———. 1995, J. Geophys. Res., 100, 14755
Beavers, W. I., & Eitter, J. J. 1986, ApJS, 62, 147
Bertin, P., Lamers, H. J. G. L. M., Vidal-Madjar, A., Ferlet, R., & Lallement, R. 1995a, A&A, 302, 899
Bertin, P., Vidal-Madjar, A., Lallement, R., Ferlet, R., & Lemoine, M. 1995b, A&A, 302, 889
Buscombe, W., & Kennedy, P. M. 1968, MNRAS, 139, 341
Duflot, M., Figon, P., & Meyssonnier, N. 1995, A&AS, 114, 269
Duquennoy, A., Mayor, M., & Halbwachs, J.-L. 1991, A&AS, 88, 281
Gaidos, E. J., Henry, G. W., & Henry, S. M. 2000, AJ, 120, 1006
Galli, A., et al. 2006, ApJ, 644, 1317
Gloeckler, G., & Geiss, J. 2004, Adv. Space Res., 34, 53
Gruntman, M., Roelof, E. C., Mitchell, D. G., Fahr, H. J., Funsten, H. O., & McComas, D. J. 2001, J. Geophys. Res., 106, 15767
Gullberg, D., & Lindegren, L. 2002, A&A, 390, 383
Hébrard, G., Mallouris, C., Ferlet, R., Koester, D., Lemoine, M., Vidal-Madjar, A., & York, D. 1999, A&A, 350, 643
Irwin, A. W., Yang, S., & Walker, G. A. H. 1992, PASP, 104, 101
Izmodenov, V. V., & Alexashov, D. B. 2003, Astron. Lett., 29, 58
Izmodenov, V. V., Lallement, R., & Malama, Y. G. 1999, A&A, 342, L13
Izmodenov, V. V., Wood, B. E., & Lallement, R. 2002, J. Geophys. Res., 107, SSH 13-1
Lallement, R., & Bertin, P. 1992, A&A, 266, 479
Lallement, R., Ferlet, R., Lagrange, A. M., Lemoine, M., & Vidal-Madjar, A. 1995, A&A, 304, 461
Linsky, J. L. 1998, Space Sci. Rev., 84, 285
Malama, Y. G., Izmodenov, V. V., & Chalov, S. V. 2006, A&A, 445, 693
McComas, D., et al. 2005, in Proc. Solar Wind 11/*SOHO* 16: Connecting the Sun and Heliosphere, ed. B. Fleck & T. H. Zurbuchen (ESA SP-592; Noordwijk: ESA), 689
Moos, H. W., et al. 2002, ApJS, 140, 3
Murdoch, K. A., Hearnshaw, J. B., & Clark, M. 1993, ApJ, 413, 349
Nidever, D. L., Marcy, G. W., Butler, R. P., Fischer, D. A., & Vogt, S. S. 2002, ApJS, 141, 503
Perryman, M. A. C., et al. 1998, A&A, 331, 81
Pourbaix, P., et al. 2002, A&A, 386, 280
Stone, E. C., Cummings, A. C., McDonald, F. B., Heikkila, B. C., Lal, N., & Webber, W. R. 2005, Science, 309, 2017
Tokovinin, A. A., & Smekhov, M. G. 2002, A&A, 382, 118
Wood, B. E., Linsky, J. L., & Ayres, T. R. 1997, ApJ, 478, 745
Wood, B. E., Linsky, J. L., Hébrard, G., Williger, G. M., Moos, H. W., & Blair, W. P. 2004, ApJ, 609, 838
Wood, B. E., Müller, H.-R., & Zank, G. P. 2000, ApJ, 542, 493
Wood, B. E., Müller, H.-R., Zank, G. P., Linsky, J. L., & Redfield, S. 2005a, ApJ, 628, L143
Wood, B. E., Redfield, S., Linsky, J. L., Müller, H.-R., & Zank, G. P. 2005b, ApJS, 159, 118
Wurz, P., Galli, A., Barabash, S., & Grigoriev, A. 2006, in AIP Conf. Proc. 858, The Physics of the Inner Heliosheath: Voyager Observations, Theory, and Future Prospects, ed. J. Heerikhuisen (New York: AIP), 269
Zank, G. P. 1999, Space Sci. Rev., 89, 413
Zank, G. P., Pauls, H. L., Williams, L. L., & Hall, D. T. 1996, J. Geophys. Res., 101, 21639